Title
Pseudoknot structures with conserved base triples in telomerase RNAs of ciliates.

Journal
Nucleic acids research, 35(18)

ISSN
0305-1048

Authors
Ulyanov, Nikolai B
Shefer, Kinneret
James, Thomas L
et al.

Publication Date
2007

DOI
10.1093/nar/gkm660

Peer reviewed

6150–6160 *Nucleic Acids Research, 2007, Vol. 35, No. 18* *Published online 7 September 2007*
doi:10.1093/nar/gkm660

Pseudoknot structures with conserved base triples in telomerase RNAs of ciliates

Nikolai B. Ulyanov[1,*], Kinneret Shefer[2], Thomas L. James[1] and Yehuda Tzfati[2]

[1]Department of Pharmaceutical Chemistry, University of California at San Francisco, San Francisco, CA 94158-2517, USA and [2]Department of Genetics, The Silberman Institute of Life Sciences, The Hebrew University of Jerusalem, Givat Ram, 91904 Jerusalem, Israel

Received July 1, 2007; Revised August 9, 2007; Accepted August 9, 2007

ABSTRACT

Telomerase maintains the integrity of telomeres, the ends of linear chromosomes, by adding G-rich repeats to their 3′-ends. Telomerase RNA is an integral component of telomerase. It contains a template for the synthesis of the telomeric repeats by the telomerase reverse transcriptase. Although telomerase RNAs of different organisms are very diverse in their sequences, a functional non-template element, a pseudoknot, was predicted in all of them. Pseudoknot elements in human and the budding yeast *Kluyveromyces lactis* telomerase RNAs contain unusual triple-helical segments with AUU base triples, which are critical for telomerase function. Such base triples in ciliates have not been previously reported. We analyzed the pseudoknot sequences in 28 ciliate species and classified them in six different groups based on the lengths of the stems and loops composing the pseudoknot. Using miniCarlo, a helical parameter-based modeling program, we calculated 3D models for a representative of each morphological group. In all cases, the predicted structure contains at least one AUU base triple in stem 2, except for that of *Colpidium colpoda*, which contains unconventional GCG and AUA triples. These results suggest that base triples in a pseudoknot element are a conserved feature of all telomerases.

INTRODUCTION

Telomeres are nucleoprotein structures that protect the ends of eukaryotic chromosomes (1). Telomerase is a ribonucleoprotein complex (RNP) that can add short DNA repeats onto telomeres and thus compensate for the losses caused by incomplete replication or degradation (2). The essential core components of this specialized enzyme are telomerase RNA (TER) and telomerase reverse transcriptase (TERT), which copies a small portion of TER, the template, onto the telomere's 3′-end. TERs are highly divergent in sequence and length even among closely related species. Based on phylogenetic covariation, secondary structure models were predicted for ciliates (3,4), vertebrates (5) and *Saccharomyces sensu stricto* species (6–9). However, only limited similarity in the general architecture of these models was observed (8,10).

The proposed secondary structure for ciliate TERs consists of four base-paired regions in most tetrahymenine ciliates (*Colpidium*, *Glaucoma* and *Tetrahymena* species) (3,11), denoted by Roman numerals I–IV (Figure 1). All *Paramecium* species have an additional helix V (12), while hypotrichous ciliates (*Euplotes*, *Sterkiella* and *Stylonichia*) and *T. paravorax* lack helix II (4,13). Nucleotides in the apical loop of stem IIIb can potentially form four base pairs outside of the stem, thus forming a PK (14). PK structures were later proposed for vertebrates (5) and yeast (15) TERs and found to be important for telomerase function (10).

The role of the PK in *T. thermophila* TER has been studied by several groups. Autexier and Greider studied telomerase activity reconstituted *in vitro* from micrococcal nuclease-treated endogenous telomerase fractions and *in vitro* transcribed TER (16). They found that mutations disrupting stem IIIa and even deleting most of the PK (76–99Δ; see Figure 1 inset for the numbering scheme) only moderately affected telomerase activity. Licht and Collins (17) reconstituted telomerase activity in rabbit reticulocyte lysate from both TER and TERT expressed *in vitro*, thus eliminating possible interference by partially digested endogenous TER. In this system, disrupting either of the two PK stems (70–86Δ or 77–98Δ) reduced telomerase activity more significantly. Further *in vitro* studies showed that the PK and stem IV are important for telomerase activity and cooperate in providing the repeat addition processivity—the ability to synthesize multiple telomeric repeats (18). Disrupting stem IIIa impaired the assembly of the telomerase RNP

*To whom correspondence should be addressed. Tel: +1 415 476 0707; Fax: +1 415 502 8298; Email: ulyanov@picasso.ucsf.edu
Correspondence may also be addressed to Yehuda Tzfati. Tel: +972 2 6584902; Fax: +972 2 6586975; Email: tzfati@cc.huji.ac.il

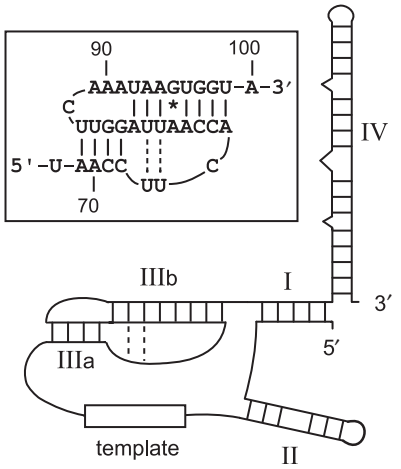

Figure 1. A schematic representation of the common secondary structure model for ciliate telomerase RNA (10). Roman numerals denote conserved base-paired regions, and open rectangle shows the template. The sequence and nucleotide numbering for the pseudoknot (PK) element in *T. thermophila* are shown in the inset. Solid vertical lines show Watson–Crick base pairs, the asterisk shows the GA mismatch and dashed vertical lines show the AUU base triples proposed here.

complexes *in vivo* and reduced the telomere length and telomerase activity assayed *in vitro* in partially purified cell extracts (19,20).

The high-resolution structure of the human TER PK has been solved by NMR (21). This structure revealed an extended triple-helical segment with base triples in the major groove of stem S2 and minor groove of stem S1, and a Hoogsteen UA pair in the junction. The triple helix within stem S2 consists of three consecutive AUU base triples, where uracils from the third strand form Hoogsteen hydrogen bonds with adenines from the duplex. A molecular model with five consecutive AUU base triples, based on extensive mutational analysis, has been proposed for the PK of the budding yeast *Kluyveromyces lactis* TER (22). Importantly, disrupting the triplex part of the PK abolished telomerase function in *K. lactis* cells, while triple compensatory mutations forming pH-dependent GCC^+ triples partially restored it.

In the current work, we analyzed PK sequences in 28 species of ciliates, belonging to seven different genera (*Colpidium*, *Euplotes*, *Glaucoma*, *Paramecium*, *Sterkiella*, *Stylonichia* and *Tetrahymena*). Based on the lengths of the stems and loops, we classified them into six morphologically different groups and calculated molecular models for representatives of each group. All ciliate sequences can potentially form at least one base triple in stem 2 of the PK. In all structures except that of *C. colpoda*, these are the conventional AUU base triples, while the latter contains unconventional GCG and AUA triples.

MATERIALS AND METHODS

Sequences

TER sequences, determined by a number of groups (3,4,11–13,23), were used as available from the GenBank (24) with the following exceptions. The sequences of *T. malaccensis*, *T. pyriformis*, *T. pigmentosa*, *T. hyperangularis*, *T. hegewishii* and *G. chattoni* were not available in the GenBank and were acquired instead from (3). For *P. primaurelia* (pseudogene B), *P. multimicronucleatum* and *P. caudatum* (strain 'JR Preer stock C-101'), some discrepancies were found between the sequences in the GenBank and the original publication; the published versions of these sequences were used (12). The TER sequence of *P. caudatum* (strain 'RB1') has not been published but is available from the GenBank (accession number AJ132318). GenBank accession numbers of all sequences used are given in Supplementary Data. Altogether, we analyzed 30 TER sequences from 28 ciliate species (*P. caudatum* has different TER sequences in two strains, and both the functional TER gene and a pseudogene are sequenced in *P. primaurelia*).

Modeling

Molecular models of PK structures were calculated using the miniCarlo program (25) on an SGI Octane R12000 computer essentially as described previously (22). miniCarlo is an internal coordinates-based program for molecular mechanics calculations of nucleic acids. The program assumes fixed values of bond lengths and fixed idealized geometries of aromatic bases. The set of internal coordinates includes generalized helical parameters that define relative positions of bases of nucleic acids in space. Flexible sugar rings are calculated using a one-parameter model (pseudorotation phase angle). A specialized chain-closure algorithm is used to calculate coordinates of the sugar-phosphate backbones connecting adjacent nucleosides (26). Conformational energy is calculated using an empirical force field optimized for nucleic acids (27,28); hydration effects are modeled with the distance-dependent dielectric constant, and nucleotides are assumed electroneutral to take into account the shielding effect of counterions. Molecular graphics representations were prepared with the UCSF Chimera (29,30) and MIDASPlus programs (31). The atomic coordinates of all calculated models are available from the authors upon request.

RESULTS

Figure 2A shows a schematic representation of a generic PK, and Figure 2B shows the structure of the AUU base triple. Standard notations for the PK stems S1 and S2 and loops L1, L2 and L3 (32) will be used below instead of the IIIa and IIIb more commonly used in the ciliates telomerase literature (compare with Figure 1). With few exceptions, loop L2 has a length of zero in the PKs of the ciliate TERs.

A search of the GenBank and published literature resulted in 30 TER sequences from 28 different species of ciliates. The PK elements were located with the help of multiple sequence alignments using CLUSTALW (33) and with the help of published alignments and secondary structures (3,4,11–13). The PK sequence of *T. thermophila* contains a stretch of two AU base pairs in stem S2 and

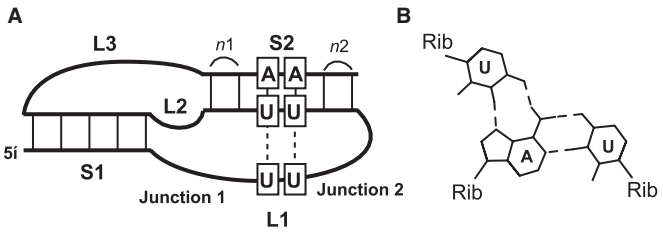

Figure 2. (**A**) A schematic representation of a generic RNA pseudoknot with stems S1, S2, loops L1, L2, L3 and AUU triples. Stems S1 and S2 correspond to stems IIIa and IIIb, respectively, in Figure 1. Vertical dashed lines show base triples formed by nucleotides of loop L1 interacting with base pairs of stem S2. Numbers of base pairs *n1* and *n2* define the position of the triple-helical segment relative to stem S2. (**B**) An AUU base triple. Hydrogen bonds are shown as dashed lines. Riboses attached to bases are indicated by 'Rib'.

two uridines in loop L1 (Figure 1). The strand direction of loop L1 is parallel to the adenines' strand. Therefore, there is a potential for forming a mini-triplex with two AUU base triples (34,35), similar to the proposed human and *K. lactis* PK structures (21,22). Inspection of PK sequences in other ciliates showed that two such triples could potentially form in most species. In *Glaucoma* and *Paramecium* species and in *T. paravorax*, there is only one such AUU triple in each PK. The only PK that cannot form any AUU triples is that of *C. colpoda*, which does not have any uridines in loop L1. Representatives of all morphologically different PK folds are listed in Table 1 and their modeling is described below. A list of all PK folds of ciliates is given in Supplementary Data.

Pseudoknot junctions

Not all arbitrary sequences forming a PK fold with AU base pairs in stem S2 and uridines in loop L2 can incorporate AUU triples. The constraints imposed by a contiguous backbone restrict the allowed combinations of the number and position of base triples, the overall size of stem S2 and the sizes of junctions 1 and 2 (i.e. residues of loop L1, which are not part of the triplex; Figure 2A). In particular, parameter $n1$ must be coordinated with the number of unpaired residues in the 5′-portion of loop L1 (i.e. with the length of junction 1), and $n2$ must be coordinated with the length of junction 2 (Figure 2A). To determine if the ciliate PK structures can accommodate base triples, we studied these requirements. Each junction was modeled separately. Figure 3A shows a model of a generic junction 1 between stem S1 and a triplex composed of six base triples as part of stem S2. Here and in other figures, stem S1 is colored gray, the Watson–Crick part of the triplex is colored orange (strand of adenines) and yellow (strand of uridines), and the third strand of the triplex (uridines) is colored cyan. An A-form of poly(A)·poly(U) was energy-minimized while preserving its heteronomous regularity (i.e. keeping identical conformations for all residues within each strand but permitting the strands to differ) and used as a model for stem S1. A heteronomous triplex poly(A)·poly(U)·poly(U) conformation was calculated in a similar way (22) and used as a model for S2. The step between stems S1 and S2 together with adjacent base pair and base triple was additionally energy-minimized. As with any hairpin-type PK, the helical twist is significantly increased at the junction (36) to juxtapose loop L1 (cyan) against the strand of adenines in stem S1. Green lines show the distance between the O3′ atom at the 3′-end of stem S1 and the O5′ atoms in consecutive residues of the third strand of the triplex in S2. These distances give estimates of the gap that needs to be filled with the residues of junction 1 for PKs with different parameters $n1$. The lower green line spans the distance that needs to be covered by the junction 1 residues if the triplex goes all the way to the bottom of stem S2 (parameter $n1 = 0$; see Figure 2A). The upper green line shows the corresponding distance in the case of $n1 = 2$. While the exact values of these distances depend on the particular conformation of the S1/S2 junction, it is clear that they grow rapidly with $n1$ value (Figure 3C, dashed line). When the backbone is intact and there are no single-stranded residues in junction 1 (as, e.g. in the *T. thermophila* sequence), this distance is ca. 2.5 Å, assuming that the O3′-P-O5′ bond angle is fixed. This means that the conformation of junction 1 will be the least strained when $n1 = 0$ and will probably be significantly modified for $n1 = 1$. For greater values of $n1$, additional unpaired residues in junction 1 of loop L1 will likely be required in order to make the PK fold able to accommodate the triplex in stem S2.

A model of a generic junction 2 is shown in Figure 3B; this junction connects the upper end of the third strand of the S2 triplex composed of three base-triples with the distal end of stem S2. This model was calculated in a manner similar to that described above. The double-stranded distal (upper) part of stem S2 (blue) is a minimized A-form of poly(A)·poly(U), and the transition between the triplex and duplex parts of stem S2 does not have prominent features; it required only minor adjustments of the conformation during energy minimization. The lower green line shows the O3′-O5′ distance between the triplex part of L1 and distal end of S2 in the case of $n2 = 3$; this distance must be covered with the unpaired residues of junction 2. Because of the double-stranded character of the upper part of stem S2, building junction 2 is somewhat similar to building an apical loop on the top of a hairpin. In this case, the two shortest spans across the major groove are for the PKs with parameters $n2 = 4$ and 5 (see Figure 3C, solid line); this is a well-known fact that follows from the geometry of A-form of RNA (37). To accommodate the triplex with $n2$ values different from 4 or 5, unpaired residues in junction 2 of loop L1 will probably be required. Results of the modeling of generic junctions 1 and 2 and analysis of the PK sequences in ciliates (Supplementary Data) indicate that morphological parameters appear to be compatible with PK structures incorporating AUU base triples in all species except *C. colpoda*. Below we show that such structures are indeed feasible. The case of *C. colpoda* will be considered separately.

Table 1. Sequences and morphological parameters of telomerase RNA pseudoknots[1]

Species	Pseudoknot sequence	Stems	Loops	Triplex	E[2]
T. thermophila (31 nt)	AAAUAAGUGGU C ***|||| UUGGAUUAACCA |||| || / 5′-AACC || C UU--/	*s*1 = 4 *s*2 = 8	*l*1 = 3 *l*2 = 0 *l*3 = 4	*t* = 2 *n*1 = 1 *n*2 = 5	−8.7
T. paravorax (25 nt)	UAUCAGGGGC A ***||| CGGGUUUCCG ||* | / 5′-GCU | / U--/	*s*1 = 3 *s*2 = 7	*l*1 = 1 *l*2 = 0 *l*3 = 4	*t* = 1 *n*1 = 1 *n*2 = 5	−8.8
G. chattoni (30 nt)	CAACAAAAGUC A |||||*| ACGGGUUUUCUG |||| | / 5′-UGCC | C U---/	*s*1 = 4 *s*2 = 8	*l*1 = 2 *l*2 = 0 *l*3 = 4	*t* = 1 *n*1 = 1 *n*2 = 6	−8.3
P. tetraurelia (25 nt)	GU-GUAGCG A ||||* CUUACAUCGU ||*| | / 5′-GAGU | / AU/	*s*1 = 4 *s*2 = 6	*l*1 = 2 *l*2 = 0 *l*3 = 3	*t* = 1 *n*1 = 2 *n*2 = 3	−7.9
E. aediculatus (39 nt)	AAAUCA--AAUCAGGC U |||||||| U-UCUCA-UUAGUCCG |||| || / 5′-AGAG || A CAUUU-/	*s*1 = 4 *s*2 = 8	*l*1 = 6 *l*2 = 1 *l*3 = 8	*t* = 2 *n*1 = 0 *n*2 = 6	−8.4
C. colpoda (29 nt)	UAAGGAAAGU U ||||| ACGGACUUUCA |||| || | | 5′-UGCC || | / GA-A/	*s*1 = 4 *s*2 = 6	*l*1 = 3 *l*2 = 1 *l*3 = 5	*t* = 3 *n*1 = 0 *n*2 = 2	−10.1
K. lactis[3] (41 nt)	U 5′-GCA AAAAUCAUU |*| ||||||*| 3′-CCAAACCU-UUUUAGUGA ||||| | |||| / 5′-GGUUU | |||| / CU-UUUU---	*s*1 = 5 *s*2 = 12	*l*1 = 6 *l*2 = 0	*t* = 5 *n*1 = 2 *n*2 = 5	−9.0
Human[4] (46 nt)	AAACAAAAAAGUCAGC C ||||||||| CCCGAC-UUUCAGUCG |||||| ||| / 5′-GGGCUG ||| C UUUU-UCU	*s*1 = 6 *s*2 = 9	*l*1 = 8 *l*2 = 0 *l*3 = 8	*t* = 3 *n*1 = 0 *n*2 = 6	n/a

[1]*s*1 and *s*2 are the lengths (in bp) of stems S1 and S2, respectively. *l*1, *l*2 and *l*3 are the lengths (in nt) of loops L1, L2 and L3, respectively. *t* is the number of triples, and parameters *n*1 and *n*2 are defined in Figure 2. In sequences, vertical lines show Watson–Crick base pairs, asterisks show mismatched pairs and double vertical lines show base triples; the alignment of the third bases in the triples is based on the purine residues from S2.
[2]miniCarlo energy of minimized conformations in kcal per mole of nucleotides.
[3]Model calculated in (22). Loop L3 has not been modeled in this structure. PK parameters are determined here taking into account the CC mismatch and ignoring the bulged-out U in stem S2.
[4]NMR structure (PDB 1YMO; 21).

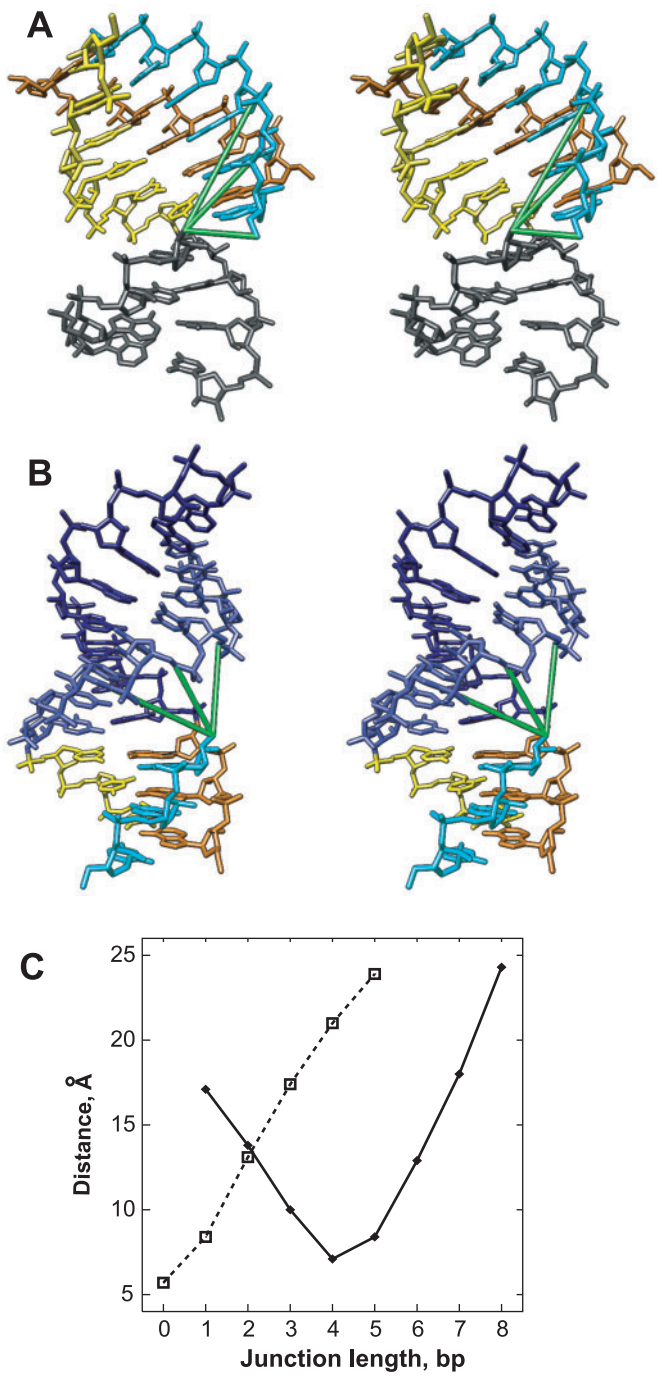

Figure 3. Pseudoknot junctions. (**A**) A stereo view of the junction between stems S1 (gray) and the triple helix formed by loop L1 (cyan) and stem S2 (orange and yellow). Green lines depict the distance between the O3′ atom at the 3′-end of stem S1 and the O5′ atoms in consecutive residues of the third strand of the triplex. Three green lines correspond to PKs with parameters $n1 = 0$, 1 and 2. (**B**) A stereo view of the junction between loop L2 participating in the triplex and the distal end of stem S2. The part of stem S2 not participating in the triplex is shown in blue: the adenine strand in dark blue and the uridine strand in light blue. Green lines show the distance between the O3′ atom at the 3′-end of the third strand of the triplex and the O5′ atoms in consecutive residues of the uridine strand of stem S2. Three green lines correspond to PKs with parameters $n2 = 3$, 4 and 5. (**C**) Dependence of the O3′-O5′ distances defined in (A) and (B) on parameters $n1$ (dashed line) and $n2$ (solid line). For definition of parameters $n1$ and $n2$, see Figure 2A.

Modeling of PK structures with AUU base triples

We modeled representative PK structures of ciliates with different morphology (Table 1), starting with the *T. thermophila* PK (Figure 4A). Briefly, individual PK components were constructed and energy-minimized; then the components were assembled, and the PK structure was again energy-minimized. Using the generic junctions modeled above, the *T. thermophila* sequence was substituted for the AU sequences in stem S1 and in the duplex-triplex combination within stem S2, and each stem was energy minimized. After that, the S1/S2 junction together with junction 1 of L1 was energy-minimized. Two uridines from L1 are aligned with two AU base pairs from S2 in such a way that one base pair of S2 separates the lower base triple from the S1/S2 junction, i.e. parameter $n1 = 1$ (Figure 4A and Table 1). This is the next to optimal alignment of base triples (the optimal is with $n1 = 0$; Figure 3C), and there are no unpaired residues in junction 1 of L1. Nevertheless, the minimized conformation of the junction accommodated the linkage between S1 and L1 with only slightly strained backbone. The backbone torsion angles zeta and epsilon between residues C72 and U73 are in the 'trans' and 'gauche-minus' minima, respectively (instead of more usual 'gauche-minus' and 'trans', respectively); also, torsion angle beta (145°) deviates somewhat from the perfect 'trans' value. Such morphology of the S1/S2 junction with $n1 = 1$ and no unpaired residues in junction 1 of L1 is conserved in most *Tetrahymena*, *Glaucoma* and *Colpidium* species (Supplementary Table S1).

Next, the unpaired residue in junction 2 of loop L1 (C75) was added to the model, and junction 2 was energy-minimized. The alignment of the upper part of the mini-triplex with respect to stem S2 is almost optimal with $n2 = 5$ (Table 1 and Figure 3C), so the position of the unpaired C75 is only slightly constrained by the requirements of the backbone closure. This residue is likely to be flexible; it was modeled as looking outwards from the helix (Figure 4A). There is a potential that C75, if protonated, forms a Hoogsteen interaction with G95 from the GA pair in stem S2 (data not shown). However, C75 is not conserved in *Tetrahymena* species (it is sometimes replaced with an A), nor is the GA mismatch conserved (Supplementary Table S1).

Finally, we modeled loop L3, shown in magenta in Figure 4A. The L3 residues were added to the model and energy-minimized. Loop L3 is certainly long enough (4 nt) to span the minor groove of the 4-bp stem S1. Similarly to the unpaired C75 from L1, loop L3 is not strongly constrained by the requirements of the backbone closure, and as a result, its conformation in the model is quite arbitrary. As is not uncommon with various PK structures, L3 residues make occasional hydrogen bonds with the minor groove side of stem S1; however, such 'minor groove triplexes' (38) do not have any regular helical conformation. In the *T. thermophila* model, A91 makes hydrogen bonds with a GC pair (between N1 of A91 and the amino group of G84 and between the amino group of A91 and O2 of C72); A90 makes a hydrogen bond with G85 (between N1 of A90 and the amino group of G85).

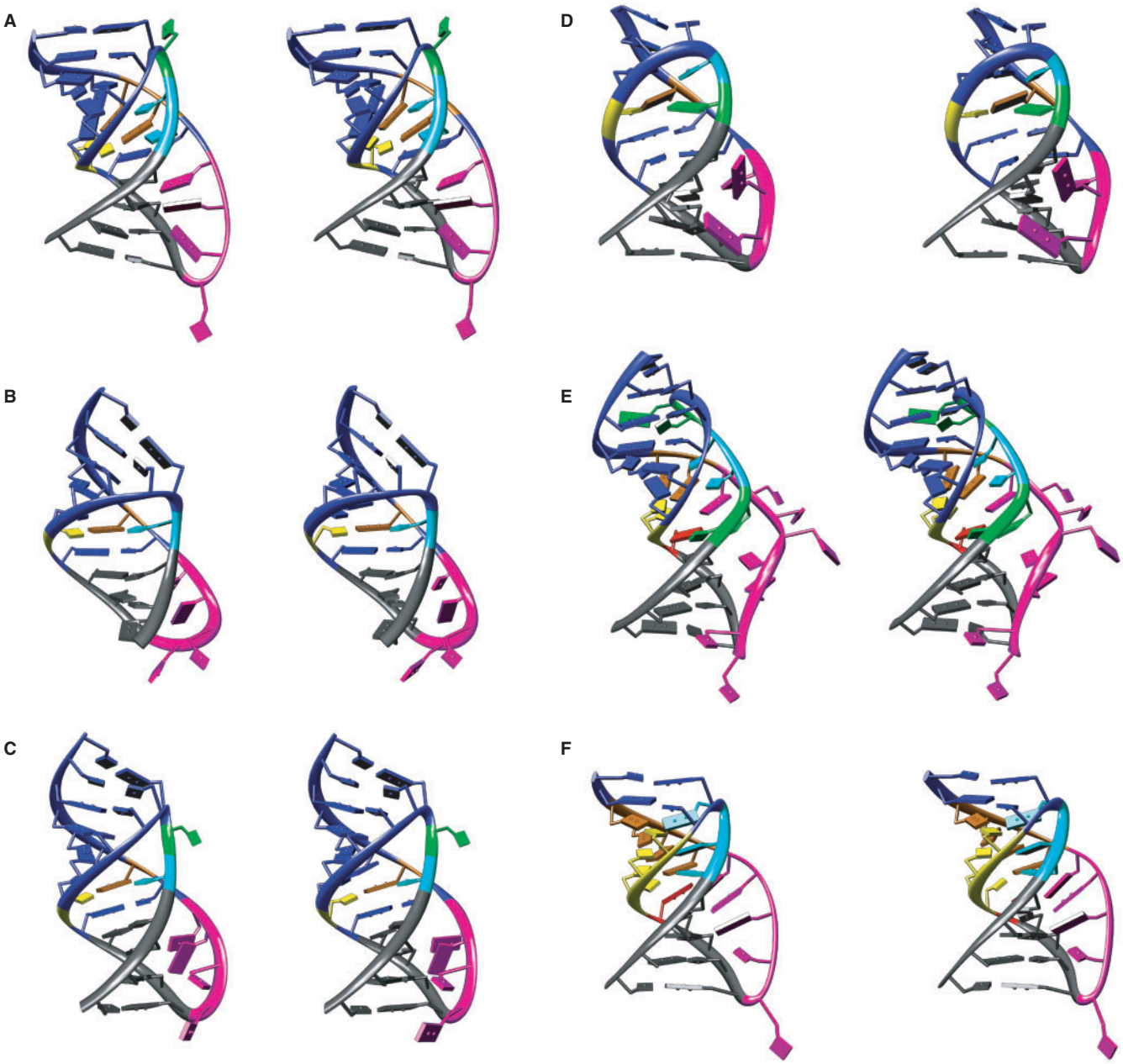

Figure 4. Ribbon representations of models of telomerase RNA pseudoknots, stereo views. Stem S1 is shown in gray. Residues of stem S2 not participating in base triples are shown in blue. Residues of stem S2 that are part of the triplex are shown in orange (purines) and yellow (pyrimidines). Residues of loop L1, which are part of the triplex, are shown in cyan; the rest of loop L1 is shown in green. Loop L2, if present, is shown in red, and loop L3, in magenta. (**A**) *T. thermophila*, (**B**) *T. paravorax*, (**C**) *G. chattoni*, (**D**) *P. tetraurelia*, (**E**) *E. aediculatus* and (**F**) *C. colpoda*.

Loop L3 is relatively A-rich, but the adenine positions are not absolutely conserved even in *Tetrahymena* species (Supplementary Table S1). Taken together with the uncertainty of the modeling of this loop, it is not clear if these specific minor groove base triples are indeed formed, and if they are conserved in ciliates. Nevertheless, in the NMR structure of the human TER PK, two adenines from loop L3 do make hydrogen bonds with the minor groove of stem S1 (21). Deletion of these adenines led to the loss of telomerase activity *in vitro* (39), suggesting that the formation of the minor groove base triples may be important.

The rest of the models were calculated in a similar way. We modeled all the morphologically different PK variants of ciliates (Table 1, Figure 4). The *T. paravorax* PK (Figure 4B) has only one AUU base triple, and shorter stems S1 and S2 than those of the *T. thermophila* PK. Similarly to *T. thermophila*, parameter $n2 = 5$; however, there are no unpaired residues in the junction 2 region of loop L1. Consequently, the backbone between L1 and

S2 is somewhat strained. Nevertheless, the loss in energy is not very high, and the total conformational energy is similar in the two *Tetrahymena* species (Table 1). Two of the sequenced *Colpidium* TER genes, *C. striatum* and *C. campylum*, have morphological PK parameters similar to those of the *Tetrahymena* species (Supplementary Data), while *C. colpoda* has a very different PK sequence and will be considered separately.

Parameter *n*2 is increased to 6 in both *Glaucoma* species (Table 1 and Supplementary Table S1), which means an increased distance between the U from L1 and the distal end of S2 that need to be connected by the backbone during model building (Figure 3C). Unlike *T. paravorax*, there is an unpaired C in junction 2 in the *Glaucoma* PKs, which partially offsets the increase in *n*2. Still, this residue is more constrained than in *T. thermophila*; as a result, it has a C2′-*endo* sugar pucker in the *G. chattoni* PK model (Figure 4C). Since there is a run of four AU base pairs in stem S2 in both *Glaucoma* species, the single U residue of L1 could align differently to S2. However, any other alignment would increase parameter *n*1, and therefore the backbone closure would not be possible in junction 1 of loop L1.

All *Paramecium* species have a distinct set of PK parameters. First, parameter *n*1 = 2 increases significantly the size of the gap in junction 1 (Figure 3C). This is compensated by an unpaired adenine in this junction, which helps fill this gap. Adenine is conserved in this position in all *Paramecium* species. In the PK model of *P. tetraurelia*, the amino group of this adenine (shown in green in Figure 4D) makes a hydrogen bond with the O4 atom of the same uracil from stem S2 that is part of the AUU triple (Figure 5A). Second, parameter *n*2 = 3 is also not optimal for junction 2 (Figure 3C). However, the closing pair of stem S2 is a wobble GU pair; the uracil is shifted in the wobble pair relative to its Watson–Crick position in the direction, which, remarkably, helps fill the gap of junction 2. This closing GU pair is conserved in all *Paramecium* species.

Euplotes, *Stylonichia* and *Sterkiella* species have longer loops L1 and L3, and they have a one-nucleotide loop L2. We modeled the PK structure of *Euplotes aediculatus* as an example of this PK morphology (Figure 4E). Similarly to other PKs with loop L2, this structure is bent (40). Since two unpaired residues are located in both junctions 1 and 2 of L1, building a contiguous backbone in this model was straightforward. Unpaired residues in junction 1 were modeled using a CpA dinucleotide platform structural motif (Figure 5B). Such a motif was first discovered for ApA dinucleotides (41), but was then extended to some other sequences as well [see, e.g. (42,43)]. To the best of our knowledge, this motif has not been discussed in the literature for CpA dinucleotides, but is nevertheless present in at least one crystal RNA structure, the large ribosomal subunit of *Haloarcola marismortui* (44) (data not shown). *Stylonichia* and *Sterkiella* species have an even longer junction 1 (three unpaired residues), which means that the PK fold with base triples is even less constrained in this case.

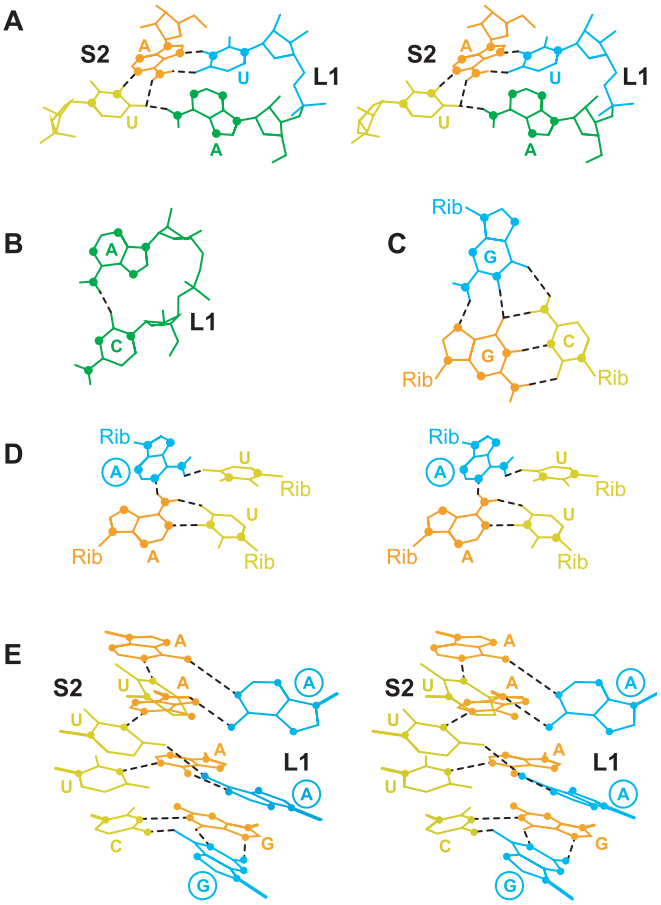

Figure 5. Structural details of the PK models. The coloring scheme is consistent with that of Figure 4. Filled circles show nitrogen atoms. (**A**) A stereo view of the interactions of loop L1 residues in the *P. tetraurelia* PK model, including the uracil participating in the AUU triple and the adenine from junction 1. (**B**) Unpaired residues of loop L1 (junction 1) of the *E. aediculatus* form a CpA dinucleotide platform motif. (**C**) An R-triple GCG from the *C. colpoda* PK model. (**D**) A stereo view of an AUA R-triple from the *C. colpoda* PK model. Note that the loop L1 adenine (label is encircled) forms hydrogen bonds with bases of two neighboring base pairs of stem S2. Ribose and phosphate atoms and the adenine from the upper AU base pair are omitted for clarity. Glycosidic bonds are denoted by 'Rib'. (**E**) A stereo view of the network of hydrogen bonds in the *C. colpoda* PK. Glycosidic bonds are shown in thicker lines. Labels for the loop L1 residues are circled. In the Watson–Crick pairs, only the central N1–N3 hydrogen bonds are shown. The orientation is ~180° relative to the view in (D).

Modeling the PK structure of *Colpidium colpoda*

The *C. colpoda* sequence is the only example of a TER PK in ciliates that cannot form AUU triples, because it does not have any uracils in loop L1. On the other hand, the L1 sequence in *C. colpoda*, GAA, is homologous to a stretch of purines in stem S2 and has the same 5′-to-3′ orientation as this stretch (Table 1). The L1 GAA bases could potentially form non-conventional purine–purine–pyrimidine triples with homologous base pairs of stem S2. Such base triples have been proposed by Zhurkin and co-workers in their model of an R-triplex, a RecA-promoted DNA triplex intermediate in homologous recombination (45). According to this model,

a single-stranded DNA can recognize a homologous DNA duplex; in particular, guanines can form so-called R-triples with GC pairs, adenines with AT pairs, and so on. We have found an example of a GCG triple in the R-type geometry in the crystal structure of the 23S rRNA (G744-G702-C726) (44), and they have also been found in other rRNA structures [see (46) and references therein]. However, we have not found any example for AUA triples in published RNA structures. The structure of the GCG triple used in the modeling of the *C. colpoda* PK is shown in Figure 5C. We calculated a model of the R-triplex GAA·GAA·UUC and used it to build the *C. colpoda* PK structure. Although the morphological parameter $n2 = 2$ (or 3, depending on the exact alignment of the third strand), the estimates shown in Figure 3C are not applicable to this structure because of the different triplex geometry and, more importantly, because of the different position of the third base relative to the base pair. Nevertheless, it was possible to build a sterically sound backbone for the PK incorporating three R-triples (Figure 4F). In fact, the conformational energy of the minimized PK model is substantially lower for *C. colpoda* than for other ciliates (Table 1), possibly because of the three base triples present in this fold. Note that the conformational energy can only be used to assess the quality of the model; it is not the free energy of the PK folding. Indeed, it has been shown that the hydrogen bonds between the third base and the Watson–Crick pair in R-triples contribute less to the free energy than the Hoogsteen hydrogen bonds (47).

During energy minimization, several conformational adjustments occurred in the *C. colpoda* PK structure. Purines from loop L1 twisted out of the planes of the base triples, and an adenine formed hydrogen bonds with two neighboring base pairs of stem S2 (Figure 5D). The base-pairing scheme shown in Table 1 is thus just a 2D simplification of a complex 3D structure. This structural feature is reminiscent of a so-called 'collapsed R-triplex' proposed by Zhurkin *et al.* (45). The last adenine of loop L1 shifted out of register and formed hydrogen bonds with a more distal AU pair of stem S2. The full network of hydrogen bonds in the triplex is shown in Figure 5E. Altogether, our modeling reveals that GCG and AUA triples can form in the *C. colpoda* PK.

DISCUSSION

When the first structure of an RNA PK was characterized by NMR, the authors noted that residues of loop L1 spanning the major groove of stem S2 could potentially form base triples (48). Later, a GCC^+ triple with a protonated cytosine was observed in a crystal structure of the frameshifting PK from the beet western yellow virus (38) and was shown to contribute to the stabilization of the PK (49). An NMR structure of the human TER PK determined by Theimer *et al.* (21) revealed an extended triple-helical region, which includes three consecutive AUU major-groove triples in stem S2. A model with a similar motif in stem S2, including five consecutive AUU triples, was proposed for the PK element in *K. lactis* TER (22). The TER sequence of another budding yeast, *Saccharomyces cerevisiae*, also appears compatible with the common structural motif of a PK that includes AUU triples (unpublished data). Although the PK formation in ciliate TERs was suggested as early as 1991 (14), the high-resolution structure of this element is still unsolved; the dynamic nature of this element in ciliates (50) has probably hindered its structural analysis. To overcome this obstacle, we undertook a computer modeling approach. By calculating molecular models of six representative folds, we demonstrated that all available ciliate TER sequences are capable of forming base triples in their PK elements. In 20 out of 30 available sequences, including that of *T. thermophila*, there are two AUU triples in this motif. In 9 sequences, including those of *T. paravorax* and all *Glaucoma* and *Paramecium* species, there is only one AUU triple, and in one species, *C. colpoda*, three unconventional purine–purine–pyrimidine base triples can potentially form. Despite significant variations in the PK sequences of ciliate TERs, the morphological parameters are balanced in such a way that can accommodate base triples in all PK folds. An example of this delicate balance is demonstrated in the *Paramecium* TER sequences with the suboptimal value of parameter $n2$. In these structures, the presence of a conserved GU wobble pair compensates for the suboptimal $n2$ value by reducing the size of the gap in junction 2.

Such a remarkable conservation of this unusual structure suggests that it contributes a conserved telomerase function. In *K. lactis*, mutations disrupting the triplex or shifting the alignment of the third strand abolished or severely impaired telomerase function. Even a relatively minor alteration of the triplex structure by substituting GCC^+ for AUU triples affected the fidelity or the processivity of the template copying *in vivo*, i.e. they led to nucleotide misincorporations and truncated telomeric repeats (22). However, the exact role of this structural element and the molecular mechanism involved remain unclear. A possible role of base triples could simply be the stabilization of the PK structure. However, there are other ways to do so, such as to lengthen its stems or replace AU with GC base pairs. The remarkable conservation of base triples in vertebrates, yeast and ciliates TER PKs, despite the widely different lengths of the PK stems (Table 1) argues against such an explanation.

Base triples could be specifically recognized by one of the telomerase proteins, such as TERT or one of the regulatory proteins, or base triples could be required for stabilization of a different binding site. Conflicting experimental data supporting or contradicting this possibility were published over the years. PK sequences were found to be required for the binding of Est2 (the yeast TERT) to the *S. cerevisiae* TER (6,8). In *T. thermophila*, the PK element appeared to be dispensable for the binding of TERT to TER *in vitro*, at least in some experiments (18). However, mutant TER sequences with disrupted stem S1 failed to form active telomerase RNP *in vivo* (19). Secondary structure probing suggested that the PK region in naked *T. thermophila* TER was rather dynamic and

unstable (50). The reconstitution of TER and TERT into an active complex *in vitro* caused a significant stabilization of the PK fold (51). This is also consistent with footprinting data: while the AAUU sequence of stem S1 and the adenines of stem S2 were accessible for modification by dimethyl sulfate in naked RNA *in vitro*, they were protected from methylation *in vivo* (52). Interestingly, the single-stranded CAAA sequence of loop L3 was also protected from methylation *in vivo*, suggesting that a protein may bind to this site or that these residues are involved in the minor-groove base triples.

It is possible that a relatively low stability of the PK is a specific feature of ciliates and may be connected to the relatively short length of stem S1 (4 bp). Indeed, our attempts to reconstitute the *T. thermophila* PK *in vitro* from two separate RNA strands were unsuccessful (unpublished data), even though similarly designed constructs formed stable dimers for the *K. lactis* sequences (22). This may also explain why the high-resolution structure for the *T. thermophila* PK has not yet been solved, despite the relatively short size of this RNA. It is not clear if this relatively low stability has a functional role, e.g. in facilitating a conformational switch, as proposed for the human PK (53). The short size of stem S1 is universally conserved in ciliates (Supplementary Table S1), supporting this notion. There is a precedent for a short RNA stem (exactly 4 bp) being important for function—the nucleocapsid protein-driven maturation of the dimerization initiation site in HIV-1 RNA (54).

Similarly to ciliates, the human PK was also suggested to be dynamic (55). The idea of the human TER PK serving as a conformational switch was introduced based on the fact that two alternative folds, the PK and a hairpin, have similar stabilities in the context of short RNA constructs (53,56). NMR structures of both the PK and the hairpin conformations have been solved (21,56). However, mutations disrupting the intra-loop base pairing in the hairpin structure did not affect the *in vitro* activity of telomerase reconstituted either *in vitro* or *in vivo* (39), casting doubt on the biological relevance of the hairpin structure. The role of such a conformational switch, if any, is unknown. One may hypothesize that it regulates the transition between different stages of the telomerase reaction cycle, enabling the processive synthesis of multiple telomeric repeats from a single template. The contribution of the PK (in cooperation with stem IV) to the processivity of the *T. thermophila* telomerase (18) is consistent with this hypothesis. In *K. lactis*, stem S2 with 5 predicted base triples is expected to be more stable while a hairpin conformation was not detected by UV melting experiments (22), arguing against a conformational switch that involves the unwinding of stem S2 in this species. Instead, a different type of a conformational switch is theoretically possible, involving a one base shift in the register of the third strand of the triplex (22). However, there is no experimental support so far for the relevance of such a conformational switch. Unlike ciliate and vertebrate telomerases, *S. cerevisiae* and *K. lactis* telomerases lack the ability to synthesize multiple repeats without dissociating from the telomeric substrate, at least *in vitro* (57,58). It is possible that the lack of repeat addition processivity is related to the absence of an alternative hairpin conformation in yeast. Another possible role for the low stability of the ciliate PK may be related to the biogenesis pathway of the telomerase RNP. *T. thermophila* TER undergoes structural rearrangement following the binding of the telomerase protein p65, which in turn enables the binding of TERT (59). It is possible that such a structural change requires the dynamic nature of the PK. Since p65 homologs or a similar folding pathway have not been found in yeast or vertebrates, such a role for the low stability of the PK may be specific for ciliates. Additional studies are needed to uncover the role of this unusual PK element with major-groove base triples, which is common to all telomerase RNAs examined.

SUPPLEMENTARY DATA

Supplementary Data are available at NAR Online.

ACKNOWLEDGEMENTS

The authors thank Zhihua Du, Noa Gil and Victor Zhurkin for careful reading of the manuscript and helpful discussions. This work was supported by the United States-Israel Binational Science Foundation (2005088 to NBU and YT) and by the National Institutes of Health (AI46967 to TLJ). The use of the University of California, San Francisco Computer Graphics Laboratory facilities was supported by the NIH (P41 RR-01081). Funding to pay the Open Access publication charges for this article was provided by the United States-Israel Binational Science Foundation (2005088).

Conflict of interest statement. None declared.

REFERENCES

1. Bertuch,A.A. and Lundblad,V. (2006) The maintenance and masking of chromosome termini. *Curr. Opin. Cell Biol.*, **18**, 247–253.
2. Autexier,C. and Lue,N.F. (2006) The structure and function of telomerase reverse transcriptase. *Annu. Rev. Biochem.*, **75**, 493–517.
3. Romero,D.P. and Blackburn,E.H. (1991) A conserved secondary structure for telomerase RNA. *Cell*, **67**, 343–353.
4. Lingner,J., Hendrick,L.L. and Cech,T.R. (1994) Telomerase RNAs of different ciliates have a common secondary structure and a permuted template. *Genes Dev.*, **8**, 1984–1998.
5. Chen,J.L., Blasco,M.A. and Greider,C.W. (2000) Secondary structure of vertebrate telomerase RNA. *Cell*, **100**, 503–514.
6. Chappell,A.S. and Lundblad,V. (2004) Structural elements required for association of the Saccharomyces cerevisiae telomerase RNA with the Est2 reverse transcriptase. *Mol. Cell. Biol.*, **24**, 7720–7736.
7. Dandjinou,A.T., Levesque,N., Larose,S., Lucier,J.F., Abou Elela,S. and Wellinger,R.J. (2004) A phylogenetically based secondary structure for the yeast telomerase RNA. *Curr. Biol.*, **14**, 1148–1158.
8. Lin,J., Ly,H., Hussain,A., Abraham,M., Pearl,S., Tzfati,Y., Parslow,T.G. and Blackburn,E.H. (2004) A universal telomerase RNA core structure includes structured motifs required for binding the telomerase reverse transcriptase protein. *Proc. Natl Acad. Sci. USA*, **101**, 14713–14718.

9. Zappulla,D.C. and Cech,T.R. (2004) Yeast telomerase RNA: a flexible scaffold for protein subunits. *Proc. Natl Acad. Sci. USA*, **101**, 10024–10029.
10. Chen,J.L. and Greider,C.W. (2004) An emerging consensus for telomerase RNA structure. *Proc. Natl Acad. Sci. USA*, **101**, 14683–14684.
11. Ye,A.J. and Romero,D.P. (2002) Phylogenetic relationships amongst tetrahymenine ciliates inferred by a comparison of telomerase RNAs. *Int. J. Syst. Evol. Microbiol.*, **52**, 2297–2302.
12. McCormick-Graham,M. and Romero,D.P. (1996) A single telomerase RNA is sufficient for the synthesis of variable telomeric DNA repeats in ciliates of the genus Paramecium. *Mol. Cell. Biol.*, **16**, 1871–1879.
13. McCormick-Graham,M. and Romero,D.P. (1995) Ciliate telomerase RNA structural features. *Nucleic Acids Res.*, **23**, 1091–1097.
14. ten Dam,E., van Belkum,A. and Pleij,K. (1991) A conserved pseudoknot in telomerase RNA. *Nucleic Acids Res.*, **19**, 6951.
15. Tzfati,Y., Knight,Z., Roy,J. and Blackburn,E.H. (2003) A novel pseudoknot element is essential for the action of a yeast telomerase. *Genes Dev.*, **17**, 1779–1788.
16. Autexier,C. and Greider,C.W. (1998) Mutational analysis of the Tetrahymena telomerase RNA: identification of residues affecting telomerase activity in vitro. *Nucleic Acids Res.*, **26**, 787–795.
17. Licht,J.D. and Collins,K. (1999) Telomerase RNA function in recombinant Tetrahymena telomerase. *Genes Dev.*, **13**, 1116–1125.
18. Lai,C.K., Miller,M.C. and Collins,K. (2003) Roles for RNA in telomerase nucleotide and repeat addition processivity. *Mol. Cell*, **11**, 1673–1683.
19. Gilley,D. and Blackburn,E.H. (1999) The telomerase RNA pseudoknot is critical for the stable assembly of a catalytically active ribonucleoprotein. *Proc. Natl Acad. Sci. USA*, **96**, 6621–6625.
20. Cunningham,D.D. and Collins,K. (2005) Biological and biochemical functions of RNA in the tetrahymena telomerase holoenzyme. *Mol. Cell. Biol.*, **25**, 4442–4454.
21. Theimer,C.A., Blois,C.A. and Feigon,J. (2005) Structure of the human telomerase RNA pseudoknot reveals conserved tertiary interactions essential for function. *Mol. Cell*, **17**, 671–682.
22. Shefer,K., Brown,Y., Gorkovoy,V., Nussbaum,T., Ulyanov,N.B. and Tzfati,Y. (2007) A triple helix within a pseudoknot is a conserved and essential element of telomerase RNA. *Mol. Cell. Biol.*, **27**, 2130–2143.
23. Shippen-Lentz,D. and Blackburn,E.H. (1990) Functional evidence for an RNA template in telomerase. *Science*, **247**, 546–552.
24. Benson,D.A., Karsch-Mizrachi,I., Lipman,D.J., Ostell,J. and Wheeler,D.L. (2006) GenBank. *Nucleic Acids Res.*, **34**, D16–D20.
25. Zhurkin,V.B., Ulyanov,N.B., Gorin,A.A. and Jernigan,R.L. (1991) Static and statistical bending of DNA evaluated by Monte Carlo simulations. *Proc. Natl Acad. Sci. USA*, **88**, 7046–7050.
26. Zhurkin,V.B., Lysov,Y.P. and Ivanov,V.I. (1978) Different families of double-stranded conformations of DNA as revealed by computer calculations. *Biopolymers*, **17**, 377–412.
27. Zhurkin,V.B., Poltev,V.I. and Florent'ev,V.L. (1980) Atom – atomic potential functions for conformational calculations of nucleic acids. *Mol. Biol. (Mosk)*, **14**, 1116–1130.
28. Poltev,V.I. and Shulyupina,N.V. (1986) Simulation of interactions between nucleic acid bases by refined atom-atom potential functions. *J. Biomol. Struct. Dyn.*, **3**, 739–765.
29. Pettersen,E.F., Goddard,T.D., Huang,C.C., Couch,G.S., Greenblatt,D.M., Meng,E.C. and Ferrin,T.E. (2004) UCSF Chimera – a visualization system for exploratory research and analysis. *J. Comput. Chem.*, **25**, 1605–1612.
30. Couch,G.S., Hendrix,D.K. and Ferrin,T.E. (2006) Nucleic acid visualization with UCSF Chimera. *Nucleic Acids Res.*, **34**, e29.
31. Ferrin,T.E., Huang,C.C., Jarvis,L.E. and Langridge,R. (1988) The MIDAS display system. *Mol. Graph.*, **6**, 13–27.
32. Jaeger,L. and Westhof,E. (1992) RNA pseudoknots. *Curr. Opin. Struct. Biol.*, **2**, 327–333.
33. Thompson,J.D., Higgins,D.G. and Gibson,T.J. (1994) CLUSTAL W: improving the sensitivity of progressive multiple sequence alignment through sequence weighting, position-specific gap penalties and weight matrix choice. *Nucleic Acids Res.*, **22**, 4673–4680.
34. Felsenfeld,G., Davies,D.R. and Rich,A. (1957) Formation of a three-stranded polynucleotide molecule. *J. Am. Chem. Soc.*, **79**, 2023–2024.
35. Chandrasekaran,R., Giacometti,A. and Arnott,S. (2000) Structure of poly(U)-poly(A)-poly(U). *J. Biomol. Struct. Dyn.*, **17**, 1023–1034.
36. Hilbers,C.W., Michiels,P.J. and Heus,H.A. (1998) New developments in structure determination of pseudoknots. *Biopolymers*, **48**, 137–153.
37. Haasnoot,C.A., Hilbers,C.W., van der Marel,G.A., van Boom,J.H., Singh,U.C., Pattabiraman,N. and Kollman,P.A. (1986) On loop folding in nucleic acid hairpin-type structures. *J. Biomol. Struct. Dyn.*, **3**, 843–857.
38. Su,L., Chen,L., Egli,M., Berger,J.M. and Rich,A. (1999) Minor groove RNA triplex in the crystal structure of a ribosomal frameshifting viral pseudoknot. *Nat. Struct. Biol.*, **6**, 285–292.
39. Chen,J.L. and Greider,C.W. (2005) Functional analysis of the pseudoknot structure in human telomerase RNA. *Proc. Natl Acad. Sci. USA*, **102**, 8080–8085; discussion 8077–8089.
40. Chen,X., Kang,H., Shen,L.X., Chamorro,M., Varmus,H.E. and Tinoco,I. Jr (1996) A characteristic bent conformation of RNA pseudoknots promotes -1 frameshifting during translation of retroviral RNA. *J. Mol. Biol.*, **260**, 479–483.
41. Cate,J.H., Gooding,A.R., Podell,E., Zhou,K., Golden,B.L., Szewczak,A.A., Kundrot,C.E., Cech,T.R. and Doudna,J.A. (1996) RNA tertiary structure mediation by adenosine platforms. *Science*, **273**, 1696–1699.
42. Harrison,A.M., South,D.R., Willett,P. and Artymiuk,P.J. (2003) Representation, searching and discovery of patterns of bases in complex RNA structures. *J. Comput. Aided Mol. Des.*, **17**, 537–549.
43. Fenn,S., Du,Z., Lee,J.K., Tjhen,R., Stroud,R.M. and James,T.L. (2007) Crystal structure of the third KH domain of human poly(C)-binding protein-2 in complex with a C-rich strand of human telomeric DNA at 1.6 A resolution. *Nucleic Acids Res.*, **35**, 2651–2660.
44. Ban,N., Nissen,P., Hansen,J., Moore,P.B. and Steitz,T.A. (2000) The complete atomic structure of the large ribosomal subunit at 2.4 A resolution. *Science*, **289**, 905–920.
45. Zhurkin,V.B., Raghunathan,G., Ulyanov,N.B., Camerini-Otero,R.D. and Jernigan,R.L. (1994) A parallel DNA triplex as a model for the intermediate in homologous recombination. *J. Mol. Biol.*, **239**, 181–200.
46. Shchyolkina,A.K., Kaluzhny,D.N., Borisova,O.F., Hawkins,M.E., Jernigan,R.L., Jovin,T.M., Arndt-Jovin,D.J. and Zhurkin,V.B. (2004) Formation of an intramolecular triple-stranded DNA structure monitored by fluorescence of 2-aminopurine or 6-methylisoxanthopterin. *Nucleic Acids Res.*, **32**, 432–440.
47. Shchyolkina,A.K., Kaluzhny,D.N., Arndt-Jovin,D.J., Jovin,T.M. and Zhurkin,V.B. (2006) Recombination R-triplex: H-bonds contribution to stability as revealed with minor base substitutions for adenine. *Nucleic Acids Res.*, **34**, 3239–3245.
48. Puglisi,J.D., Wyatt,J.R. and Tinoco,I. Jr (1990) Conformation of an RNA pseudoknot. *J. Mol. Biol.*, **214**, 437–453.
49. Nixon,P.L. and Giedroc,D.P. (2000) Energetics of a strongly pH dependent RNA tertiary structure in a frameshifting pseudoknot. *J. Mol. Biol.*, **296**, 659–671.
50. Bhattacharyya,A. and Blackburn,E.H. (1994) Architecture of telomerase RNA. *EMBO J.*, **13**, 5721–5731.
51. Sperger,J.M. and Cech,T.R. (2001) A stem-loop of Tetrahymena telomerase RNA distant from the template potentiates RNA folding and telomerase activity. *Biochemistry*, **40**, 7005–7016.
52. Zaug,A.J. and Cech,T.R. (1995) Analysis of the structure of Tetrahymena nuclear RNAs in vivo: telomerase RNA, the self-splicing rRNA intron, and U2 snRNA. *RNA*, **1**, 363–374.
53. Comolli,L.R., Smirnov,I., Xu,L., Blackburn,E.H. and James,T.L. (2002) A molecular switch underlies a human telomerase disease. *Proc. Natl Acad. Sci. USA*, **99**, 16998–17003.
54. Mujeeb,A., Ulyanov,N.B., Georgantis,S., Smirnov,I., Chung,J., Parslow,T.G. and James,T.L. (2007) Nucleocapsid protein-mediated maturation of dimer initiation complex of full-length SL1 stemloop of HIV-1: sequence effects and mechanism of RNA refolding. *Nucleic Acids Res.*, **35**, 2026–2034.

55. Antal,M., Boros,E., Solymosy,F. and Kiss,T. (2002) Analysis of the structure of human telomerase RNA in vivo. *Nucleic Acids Res.*, **30**, 912–920.
56. Theimer,C.A., Finger,L.D., Trantirek,L. and Feigon,J. (2003) Mutations linked to dyskeratosis congenita cause changes in the structural equilibrium in telomerase RNA. *Proc. Natl Acad. Sci. USA*, **100**, 449–454.
57. Cohn,M. and Blackburn,E.H. (1995) Telomerase in yeast. *Science*, **269**, 396–400.
58. Fulton,T.B. and Blackburn,E.H. (1998) Identification of Kluyveromyces lactis telomerase: discontinuous synthesis along the 30-nucleotide-long templating domain. *Mol. Cell. Biol.*, **18**, 4961–4970.
59. Stone,M.D., Mihalusova,M., O'Connor,C.M., Prathapam,R., Collins,K. and Zhuang,X. (2007) Stepwise protein-mediated RNA folding directs assembly of telomerase ribonucleoprotein. *Nature*, **446**, 458–461.